DESIGN OF REGENERATIVE ANTI−LOCK BRAKING SYSTEM CONTROLLER FOR 4 IN−WHEEL−MOTOR DRIVE ELECTRIC VEHICLE WITH ROAD SURFACE ESTIMATION

Andrei Aksjonov[1)], Valery Vodovozov[2)*], Klaus Augsburg[3)] and Eduard Petlenkov[4)]

[1)]SKODA AUTO a.s., Tr. Vaclava Klementa 869, Mlada Boleslav 29301, Czech Republic
[2)]Department of Electrical Power Engineering and Mechatronics, School of Engineering, Tallinn University of Technology, Tallinn 19086, Estonia
[3)]Automotive Engineering Group, Department of Mechanical Engineering, Technische Universität Ilmenau, Ilmenau 98693, Germany
[4)]Department of Computer Systems, School of Information Technologies, Tallinn University of Technology, Tallinn 19086, Estonia

(*Received date ; Revised date ; Accepted date*)

ABSTRACT–This paper presents a regenerative anti−lock braking system control method with road detection capability. The aim of the proposed methodology is to improve electric vehicle safety and energy economy during braking maneuvers. Vehicle body longitudinal deceleration is used to estimate a road surface. Based on the estimation results, the controller generates an appropriate braking torque to keep an optimal for various road surfaces wheel slip and to regenerate for a given motor the maximum possible amount of energy during vehicle deceleration. A fuzzy logic controller is applied to fulfill the task. The control method is tested on a four in−wheel−motor drive sport utility electric vehicle model. The model is constructed and parametrized according to the specifications provided by the vehicle manufacturer. The simulation results conducted on different road surfaces, including dry, wet and icy, are introduced.

KEY WORDS : Fuzzy control, Anti-lock braking system, Electric vehicles, Vehicle dynamics, Vehicle safety

NOMENCLATURE

ω : wheel angular speed, rad/s
a_{vx} : vehicle longitudinal acceleration, m/s^2
p_b : braking pressure, bar
r : wheel radius, m
m : mass of the quarter vehicle, g
g : gravitational acceleration, m/s^2
T_d : driving torque, Nm
T_t : tire torque, Nm
T_b : total braking torque, Nm
T_{RB} : regenerative brake torque, Nm
T_{FB} : friction brake torque, Nm
I_w : inertia about the wheel rotational axis, gm^2
k_b : braking coefficient
T_j : phase torque of motor, Nm
I_j : phase current of motor, A
θ : rotor aligned position of motor, °
L : phase bulk inductance of motor, H
N : number of phases of motor
v_{vx} : vehicle longitudinal velocity, m/s
v_{wx} : wheel longitudinal velocity, m/s
λ : wheel slip, %
μ : tire−road friction coefficient
μ* : estimated road surface
F_x : longitudinal force, N
F_z : vertical force, N
E_c : net energy consumption, kJ
P_d : power spent on driving, W
P_b : power recovered via regenerative braking area, W

* *Corresponding author*. e-mail: valery.vodovozov@ttu.ee

η_m : electric motor efficiency, %

s : distance, m

$a_{average}$: average deceleration, m/s^2

ABS_{IP} : ABS operation index of performance

$\lambda_{average}$: average wheel slip, %

λ_e : actual and optimal wheel slip difference absolute value, %

P_{reg} : regenerated power comparing to the total power required for deceleration, %

SUBSCRIPTS

i : subscript for each wheel; $i \in$ [front left (FL), front right (FR), rear left (RL), rear right (RR)]

j : switched reluctance motor phase number

ABBREVIATIONS

4WD	4 in-Wheel-motor Drive
ABS	Antilock Braking System
ASM	Automotive Simulation Models™
DOF	Degree of Freedom
ESP	Electronic Stability Program
EV	Electric Vehicle
FLC	Fuzzy Logic Controller
ICE	Internal Combustion Engine
MF	Membership Function
MISO	Multiple Input, Single Output
PID	Proportional−Integral−Derivative
SRM	Switched Reluctance Motor
SUV	Sport Utility Vehicle
UOD	Universe of Discourse

1. INTRODUCTION

Modern life cannot be imagined without personal vehicles. As the cities grow bigger and business spread wider, people daily pass long distances to their work places or to meet with their business partners in other cities or even other countries. On−ground vehicles have become indispensable machines helping people in overcoming distances and saving time on transportation.

The world population increases every year and a demand for personal vehicles grows in parallel. Within only few past decades the number of internal combustion engine (ICE) cars has dramatically enlarged on the roads. It brings in this connection the biggest disadvantage of a developed industry: the risk of accidents and consequent human fatalities. Thus, a vehicle safety and driving assistance systems' improvement and development is needful. Moreover, the problems related to energy management, oil crisis, greenhouse gases, pollution and environment protection have brought a necessity to create a new type of environmental friendly transport. One of the promising alternatives are the electric vehicles (EV), where an ICE is replaced with an electric motor propulsion system (Bansal, 2005). EVs are not only less polluting, efficient and cheap to operate, but also very quiet (Dhameja, 2002).

The EV batteries' long recharging time, poor durability, weight, cost and short lifetime are causing the largest resistance to the EV mobility infrastructure development (Dhameja, 2002). The biggest drawback of the commercial EVs is their short range due to a small charge capacity.

One of the subtypes of an EV has four in−wheel−motor drives (4WD) powertrain. The technology was already available in 1900, when the great inventor and engineer Ferdinand Porsche introduced a vehicle with wheel hub motors built into steered front wheels. Unfortunately, the mass production failed due to the invention technical complexity.

With the technologies available today, the 4WD powertrain EVs once again deserve an attention, because they turn out to be perfect candidates for future mobility. Each of the individual 4WD motors' angular velocity and torque can be directly measured. Furthermore, the electric actuator works faster than a conventional hydraulic system used nowadays in ICE vehicles. It opens an opportunity to design a very rapid, efficient and accurate algorithm to control vehicle dynamics via 4WD powertrain (Xiong and Yu, 2011).

The well−known safety systems are an antilock braking system (ABS) and an electronic stability program (ESP). The ABS avoids wheel lock and maintains vehicle steerability (Koch−Dücker and Papert, 2014). The ESP assists in vehicle stability control (Ehret, 2014). The ABS available in commercial vehicles requires a wheel slip threshold that guarantees energy efficient deceleration only on a dry asphalt surface (Koch−Dücker and Papert, 2014). Consequently, it leads to power losses on lower adhesive coefficient surfaces, because the wheel slip requirements are lower on a slippery surface than on a dry road (Doumiati *et al.*, 2013).

In EV, the negative torque from braking inertia rotates the motor in opposite to traction direction. The motor works as a generator and charges an energy

storage device by converting kinetic energy created by the vehicle mass into an electric power, instead of wasting it as a heat on the brake pads or into the atmosphere (Miller, 2005; El−Garhz *et al*., 2013). This process is known as regenerative braking or energy recuperation (Dhameja, 2002). Kinetic energy recycled from braking maneuvers increases the EV driving distance. Thus, an ABS for EVs has a benefit for safety and efficiency improvement via regenerative braking and a challenge for more complex braking control methods design.

This work's aim is to combine the torque blending technique together with a control of robust to different road surfaces ABS. The generators use maximum power as the actuators for the ABS system. The controller recognizes the road surface to maintain energy efficient and safe braking performance for a specific road. Hence, the controller recuperates maximum possible kinetic energy from braking and simultaneously supports robust to various roads vehicle safety deceleration.

The paper is organized as follows. In next Section, the related to this studies works are analyzed and the current paper contribution is discussed. The 4WD EV powertrain modelling and parameterization are introduced in Section 3. The detailed explanation of the road detection algorithm as well as the control method description are presented in Section 4. In Section 5, the control results for different road adhesions are introduced. A comparative analysis of the controller performance for electric and hydraulic actuators is also reported. The research is discussed and concluded in Sections 6 and 7, respectively.

2. RELATED WORKS

Many different conventional control methods were proposed for EV energy regeneration. For instance, in (Long *et al*., 2014), the sliding mode controller (SMC) and the proportional−integral−derivative (PID) controllers were compared. There, the SMC outperformed the PID. In (Ye *et al*., 2010), H_2 optimal control and H_∞ robust control were combined to guarantee EV recuperation performance and stability. Those methods require very complex numerical models. Mathematical models are computationally intensive and have complex stability problems. Moreover, models are often not accurate due to approximations, uncertainty, and lack of perfect knowledge. Fuzzy logic has an advantage over conventional control techniques (e.g. PID, SMC, H_∞), because it does not require a complex dynamic model development. Hereupon, it has a benefit in processing and mapping ill-defined and uncertain variables. Consequently, within few last decades, a fuzzy logic controller (FLC) deserved special attention in complex, imprecise nonlinear control (Passino and Yurkovich, 1998 (pp. 1−22); Reznik, 1997).

One of the first EV regenerative antiskid braking and traction control system applying FLC with the tire−road adhesive characteristic estimation was proposed in (Cikanek, 1994). The controller was designed for a single-axle drive EV architecture. Since then, many other rule−base approaches were proposed for regenerative braking enhancement.

An FLC was applied to control an EV ABS with optimal wheel slip for varying road surfaces (Kathun *et al.*, 2003; Chen *et al*., 2010). In addition to robust ABS, the authors in (Pusca *et al.*, 2004; Tahami *et al*., 2003) also studied an ESP regulation. Although the controller showed precise road adhesive coefficient estimation, the authors did not investigate regenerative braking and torque blending.

Vehicle stability control for a 4WD hybrid EV was stressed in (Kim *et al*., 2008). The FLC compensated the yaw dynamics control and recycled kinetic energy. Nevertheless, the simulation results are limited to the yaw rate and side slip angle compensation.

Fuzzy set theory also deserved an attention in kinetic energy recuperation. The scholars in (Paterson and Ramsay, 1993; Peng, 2006; Li *et al*., 2008) proposed an electric motor and friction braking torque blending based on FLC. Furthermore, in (Nian, 2014), the FLC and PID control were combined to distribute the mechanical and electrical braking forces. Even so, the authors neither consider braking torque between rear and front wheels distribution nor ABS control design.

On the contrary, in (Zhang *et al*., 2016; Jianyao *et al*., 2015; Xu *et al*., 2011), the authors examine both EV torque blending and braking force allocation between EV wheels. Nevertheless, the slip control and ABS safety investigation were not presented. Further, in (Zhang *et al*., 2016), the researchers demonstrated effectiveness and strong robustness in EV energy recuperation of the Takagi−Sugeno fuzzy SMC over conventional PID and Mamdani's type FLC. The results were verified in simulation and experimentation. Though, vehicle safety was not stressed. Optimal braking torque distribution with regenerative capability was examined on vehicle stability for a single line change in (Kim *et al*., 2007) but an ABS controller was not designed there.

A regenerative ABS controller was built by combining FLC and SMC in (Guo *et al*., 2014). The intelligent regulator requires a reference slip threshold, which likewise in modern industrial vehicles lead to energy losses on other than dry road surfaces.

Fuzzy set theory is also widely used as an estimator of vehicle states, for instance, linear velocity, battery performance, vehicle side slip angle, tire−road interaction parameters (Ivanov, 2015) and tire forces

(Acosta and Kanarachos, 2017). Tire−road surface estimation with ABS control based on FLC was designed in (Layne *et al*., 1993). The goal of the controllers was to keep the slip ratio to 20% despite road friction characteristics.

In (Paul *et al*., 2016), the researchers went further and offered, first, to estimate the road surface with fuzzy logic, and therefore to provide a braking torque distribution. The controller was tested on a single motor EV model. The wheel slip and vehicle steerability were not studied on different road surfaces, because the controller is designed with a fixed slip value.

Advanced FLCs for road type detection and thus optimal braking pressure generation were designed in (Ivanov *et al*., 2006; Aly, 2010; Castillo *et al*., 2016). Although the experimental results showed perfect performance on varying road surfaces, the control algorithms are very complex. What is more, the FLCs were not tested on EV decoupled braking system, but only on conventional hydraulic brakes.

Other efficient techniques for vehicle states estimation were proposed before. Kalman filtering is widely used in vehicle longitudinal force estimation (Doumiati *et al*., 2013). Lyapunov stability theory (Xia *et al*., 2016), a combination of stiffness based estimation and least squares (Han *et al*., 2015) and a combination of nonlinear Lipschitz observer and modified super-twisting algorithm (Rath, *et al*., 2015) were designed for road friction coefficient estimation. Those methods, however, require complicated nonlinear models or additional sensors, what multiply system's cost and complexity.

In this paper, a simple method for road surface recognition is presented. The estimation is based only on vehicle body maximum deceleration rate. The proposed technique is fulfilled with FLC and, unlike other methods mentioned in this Section, requires neither complicated mathematical model nor additional sensors, because the longitudinal acceleration measurement sensors are already in use in modern vehicles (Zabler, 2014). What is more, the FLC is able to compensate the lack of knowledge about many other road surfaces that are not preliminary considered.

Previously, the road surface estimation strategy and ABS control were tested on hydraulic brake model (Aksjonov *et al*., 2016). On the contrary, in this paper, the FLCs are designed for both electric and hydraulic actuators that are interacted together. The proposed controllers' task is to maximize energy recuperation from the vehicle deceleration maneuver. Hereupon, the same FLCs ensure the robustness to different road surfaces by maintaining an optimal wheel slip during the whole braking process and by avoiding a reference slip control. Therefore, an energy efficient torque blending and road surface estimation are implemented in the same controller without complex vehicle models.

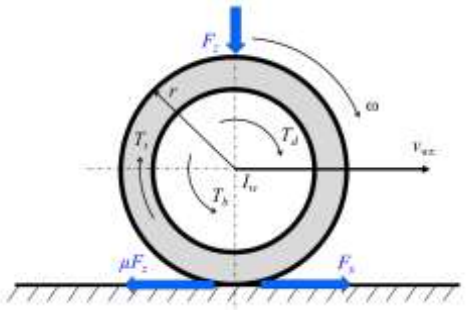

Figure 1. Vehicle single–wheel model of a braked wheel schematic drawing.

In short, the following problems are solved:

- road surface detection from vehicle body longitudinal acceleration with vehicle energy efficient deceleration due to optimal wheel slip control and maximum energy regeneration capability using fuzzy set theory;
- controller implementation on ten degree of freedom (10DOF) 4WD EV model;
- control method robustness to different road surfaces demonstration and comparison with only friction and braking with blocked wheels.

3. VEHICLE MODELLING

3.1. Dynamics of a Braked Wheel

The 3DOF single−wheel vehicle model for the EV longitudinal motion (Figure 1) is described by the following system of equations (Kiencke and Nielsen, 2005):

$$\begin{cases} I_w \cdot \dot{\omega} = T_d - T_t - T_b \\ F_x = m \cdot \dot{v}_{vx} \\ F_z = m \cdot g \end{cases} \quad (1)$$

where the tire torque T_t is expressed as:

$$T_t = r \cdot F_x \quad (2)$$

Due to its small influence comparing to the braking and friction forces during braking maneuvers, other forces, like aerodynamic drag and lateral wind force, are neglected.

A distinctive feature of the 4WD EV: total braking torque T_b is a sum of regenerative brake T_{RB} and friction brake T_{FB} torques:

$$T_b = T_{RB} + T_{FB} \tag{3}$$

where the friction brake torque is determined as (Kiencke and Nielsen, 2005):

$$T_{FB} = r \cdot k_b \cdot p_b \tag{4}$$

In turn, the friction braking coefficient k_b depends on brake disc friction area, mechanical efficiency of brake components, and braking factor. Tire deformation (change of the wheel radius r) due to its small impact is neglected. Thus, both variables r and k_b are assumed as constants. The friction braking torque changes proportionally to the brake pressure p_b.

Finally, in case of a saturated phase, a torque T_j equation for switched reluctance motor (SRM) can be given as (Ehsani *et al*., 2005) (pp. 204−232):

$$T_j = \int_0^{I_j} \frac{\partial L(\theta, I_j)}{\partial \theta} I_j dI_j \tag{5}$$

The output torque of an SRM in traction or regenerative modes $T_{d/RB}$ is the summation of torques in all the phases (Ehsani *et al*., 2005) (pp. 204−232):

$$T_{d/RB} = \sum_{j=1}^{N} T_j \tag{6}$$

The input to the SRM drive is direct current voltage. However, a convertor controls phase current I_j flow. Therefore, control of the phase torque depends directy on I_j (Ehsani *et al*., 2005) (pp. 204−232).

In modern vehicles, the torque of the vehicle wheel cannot be measured, but only estimated. On the contrary, both p_b and I_j can be measured by appropriate sensors (Zabler, 2014). In this paper, the wheel torques are controlled by influencing on p_b and I_j. The variables serve as the controller correcting variables. Nevertheless, they will be directly expressed as the relevant torques.

For the braking maneuver the longitudinal wheel slip λ is expressed as (Kiencke and Nielsen, 2005):

$$\lambda = \frac{v_{vx} - v_{wx}}{v_{vx}} \cdot 100\% \tag{7}$$

where the longitudinal wheel velocity v_{wx} is:

$$v_{wx} = r \cdot \omega \tag{8}$$

Tire deformation depends on a normal force F_z (Pacejka, 2006). The wheel radius r is assumed as constant.

Tire−road adhesive coefficient μ is determined as a ratio between longitudinal F_x and vertical F_z forces applied on a wheel (Kiencke and Nielsen, 2005):

$$\mu = \frac{F_x}{F_z} \tag{9}$$

From the single−wheel dynamics, Eq. (1), μ can be simplified as:

$$\mu = \frac{F_x}{F_z} = \frac{m \cdot \dot{v}_{vx}}{m \cdot g} = \frac{\dot{v}_{vx}}{g} \tag{10}$$

Two main variables, the vehicle longitudinal acceleration a_{vx} and the wheel angular velocity ω_i, serve as the controller inputs. The input signals are measured by the available on board sensors (Zabler, 2014). In this paper, μ is connected to maximum vehicle acceleration rate a_{vx} (Eq. (10)) for road surface recognition. The detected road surface is defined as μ*.

An overall motor power $P_{d/b}$ with motor efficiency η_m expended on driving or braking is as follows (Ehsani *et al*., 2005) (pp. 277−298):

$$P_{d/b} = \eta_m \cdot T_{d/b} \cdot \omega_i \tag{11}$$

Electric motor net energy consumption E_C is described by an equation of power spent on driving and recycled during the regenerative braking, if the last one is applied (Ehsani *et al*., 2005) (pp. 99−116):

$$E_C = \int_{traction} P_d dt + \int_{braking} P_b dt \tag{12}$$

The index of performance ABS_{IP} is introduced to evaluate the effectiveness of the ABS control. It describes the ratio between vehicle deceleration with and without the applied controller:

$$ABS_{IP} = \frac{a_{ABS}}{a_{skid}} \tag{13}$$

Table 1. Electric vehicle configurations.

Components	Parameters	Desription
Vehicle	Type	Sport utility vehicle
	Vehicle overall mass	2117 kg
	Front axle suspension spring constant stiffness	26700 N/m
	Rear axle suspension spring constant stiffness	23000 N/m
	Front axle suspension stabilizer stiffness	2851.4 N/m
	Rear axle suspension stabilizer stiffness	6833.5 N/m
	Tire type	235/55 R19
	Tire numerical model	Pacejka's Magic Formula
Electric motor	Type	Switched reluctance
	Peak torque at 800V (+/− 10%)	200 Nm (30 sec)
	Peak power at 800V (+/− 10%)	100 kW (30 sec)
	Nominal torque at 800V (+/− 10%)	125 Nm
	Nominal power at 800V (+/− 10%)	42 kW
	Maximum speed	15000 rpm
	Motor inertia (without gearbox)	21087 kgmm^2
	Mass	50 kg
	Motor dimension	215x265 mm
	Liquid cooling system	Water 10 l/min, 50° C max inlet
Transmission (in−wheel motor)	Type	Two stage reducer with helical gear and half−shaft
	Overall motor−gear ratio	1:10.5
	Estimated torsion stiffness of half−shaft	6500 Nm/rad
Battery pack	Voltage	400 V DC
	Peak power	160 kW
	Nominal power	80 kW
	Mass	274 kg
	Volume	0.235 m^3
	Energy capacity	15 Ah (6 kWh)
	Module type	12 lithium−titanate oxide anode cells
	Modules number	15

3.2. Vehicle Modelling and Parametrization

Full 10DOF vehicle mathematical model Automotive Simulation Models™ (ASM) 2014−B (64−bit) is supplied by the dSPACE® GmbH (Paderborn, Germany). The ASM allow a vehicle model parameterization according to the user's needs. The ASM interaction with the MATLAB®/Simulink® (Natick, MA, USA) R2013b (64 Bit) allows removing or substitution of the vehicle component models, if necessary. Furthermore, the control algorithm can be easily designed and simulated in MATLAB® environment without any supplementary software requirements. A multibody vehicle model simulation is accompanied with a visual interface, what help user to understand vehicle behavior in details. The EV and its powertrain system configurations are provided by a vehicle manufacturer and presented in Table 1.

The studied EV model was parametrized as a sport utility vehicle (SUV). Its total body weight is 2117 kg. Each 4WD powertrain motor is connected to the wheel through a gearbox and a half−shaft transmission. In Figure 2, a simplified in−wheel motor architecture and a controller are introduced. The EV has a decoupled electro−hydraulic brake system. Friction and electric motor brakes impacting on braking pressure and the motor phase current can be controlled independently.

Vehicle deceleration is a very fast process. In regenerative braking, huge amount of energy is released within a very short time. Most of the EV batteries are not able to save this energy. Despite, ultracapacitors are characterized by very high power, excellent life cycle, but represent a low−capacity energy storage. Consequently, most of the modern EVs are also

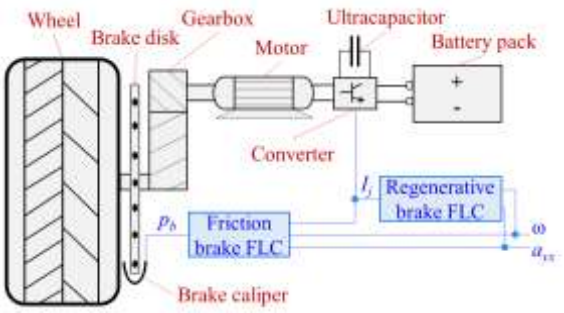

Figure 2. In–wheel motor architecture scheme: black – hardware; blue – software.

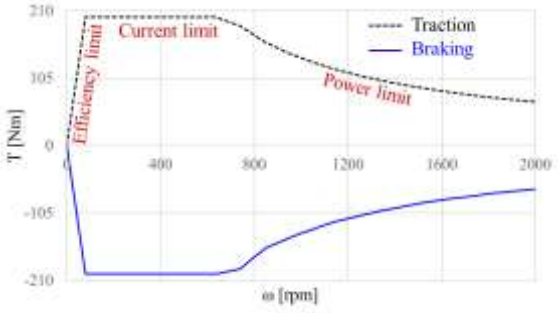

Figure 3. Torque – rotational speed characteristic for SRM in motoring and regeneration modes.

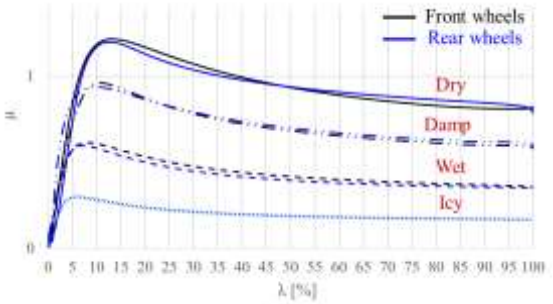

Figure 4. Tire–road friction – slip curves of the studied tire model for various road surfaces using Magic Formula model (Pacejka, 2006).

equipped with ultracapacitors used in regenerative braking for fast energy storing (Bansal, 2005). The power electronics losses are neglected in the model.

Lithium−titanate battery is used as an energy storage device. Its maximum energy capacity is 6 kWh and a peak power reaches 160 kW. Wheels are equipped with a SRM. The SRM's maximum torque that can be applied during 30 seconds at 800 V voltage in both motor and generator modes is 200 Nm. The torque versus angular speed relation for the studied SRM is shown in Figure 3. Taking into consideration the in−wheel motor overall transmission gear ratio, the maximum torque applied directly to the wheel reaches 2100 Nm (Savitski *et al.*, 2016).

A first−order transfer function describes the electric motor dynamics as follows (Savitski *et al.*, 2014, 2016):

$$\frac{T_d^{act}}{T_d^{ref}} = \frac{1}{0{,}0022s+1} e^{-0{,}002s} \tag{14}$$

whereas the motor transfer function in generator mode while braking is as follows:

$$\frac{T_b^{act}}{T_b^{ref}} = \frac{1}{0{,}02s+1} e^{-0{,}025s} \tag{15}$$

The tires are modelled with the Pacejka's Magic Formula (Pacejka, 2006). Before designing the controller, the tire characteristics were studied. To this regard, the vehicle model was simulated on dry, damp, wet, and icy road surfaces. An ABS control was not applied. The vehicle decelerates under heavy braking conditions with locked wheels.

The tire−road friction μ versus the wheel slip λ are plotted (Figure 4) to specify the stable working range for the given tire. Since the meaning of the vehicle body deceleration curves on different road surfaces is the same as the μ – λ curves, they are not introduced in this paper. Only the straight road braking maneuver is studied, a slip angle effect on tire dynamics is omitted.

Table 2. Optimal wheel slip values and vehicle body maximum deceleratin rate for different road surfaces.

λ [%]	Dry road	Damp road	Wet road	Icy road
Front wheels	13.18	10.66	8.34	6.14
Rear wheels	12.31	9.54	7.12	5.82
Peak deceleration [m/s²]	11.78	8.79	5.89	2.96

Tire dynamics have an exponential behavior (Figure 4). The optimal slip lays on the curve's peak, where the adhesive coefficient has its maximum rate. The plot region from 0 to optimal slip value is called stable for each road surface, where the vehicle maintains steerability. The rest of the curve from optimal to 100% slip is called unstable zone, where the vehicle lateral control (steerability) is impossible. Moreover, the vehicle maximum deceleration on a given road surface is achieved only with the optimal wheel slip. Braking with the slip ratios higher or lower than the optimum value leads to braking force reduction (Rajamani, 2012).

Although the vehicle velocity and tire models are the same for the front and rear wheels, the μ – λ curves are slightly different (Figure 4). This can be explained by unequal body mass and, therefore, normal force distribution between the front and rear wheels (Rajamani, 2012). Vehicle vertical load has an impact on a tire dynamic behavior (Pacejka, 2006), because friction coefficient depends on a normal force, Eq. (9).

Each road surface for the front and rear wheels of the EV has its own optimal slip. The optimal value maintenance leads to the most effective and energy efficient braking performance. Due to the forces balance, the vehicle decelerates as fast as feasible at the same time presuming the lateral control (Koch−Dücker and Papert, 2014). With the reference to the plots in Figure 4, the optimal slip values are concluded in Table 2. The peak vehicle deceleration values on different roads are also introduced in Table 2. The data are essential details for the control method design described in next Section.

4. CONTROL METHOD

4.1. Control Method Description

Regenerative ABS control algorithm has several requirements: (i) fast vehicle deceleration, (ii) vehicle steerability preservation, (iii) maximum energy recuperation rate. First two requirements are fulfilled with the wheel slip control. Efficiency of the ABS can be dramatically improved by holding an optimal wheel

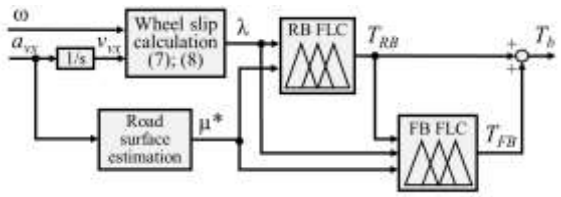

Figure 5. Single wheel controller block scheme: RB FLC – regenerative braking fuzzy logic controller; FB FLC– friction braking fuzzy logic controller; 1/s – integrational operation.

slip for a given tire on different road surfaces. The third requirement is satisfied by braking using the torque generated by an SRM only. This torque may not be enough to preserve the required slip and fast vehicle deceleration. Hence, the controller must involve a friction braking system in series while using the electric motor as a generator.

In this work, an improvement of ABS performance is proposed for the 4WD EV by keeping the wheel slip on its optimal level for various roads. For this, the algorithm uses vehicle body longitudinal deceleration to comprehend which kind of road is behind the tires. Additionally, the controller employs the electric motor for energy recuperation on its maximum power and therefore recycles as much energy as possible.

The regenerative−friction decoupled ABS control block scheme for a single wheel is presented in Figure 5. The idea is very simple: the controller uses electric motor torque and retains vehicle deceleration with an optimal slip ratio for a given road. The mechanical friction brake system is activated only when the generator's torque is not enough to maintain the optimal slip. In fact, the controlled parameters are phase current for the regenerative brakes and the brake caliper pressure for the friction brakes. For better understanding, the outputs are expressed directly as appropriate torques.

Displacement of a braking pedal activates the ABS controller. The safety feature is deactivated when the braking pedal is released or vehicle velocity is smaller than 8 km/h, because a distance travelled with the locked wheels from 8 km/h is not critical for vehicle safety (Koch−Dücker and Papert, 2014).

An integrated signal transmitted from a vehicle longitudinal acceleration a_{vx} sensor and a signal from a wheel speed ω_i sensor are used to estimate a tire slip for each wheel λ_i. The same estimation approach is used in modern vehicles (Koch−Dücker and Papert, 2014). The method is assumed to be enough accurate as the sensors offset, noise, and integration drift have no dramatic influence on λ calculation. A side slip influence can be also neglected, because only straight braking maneuver is performed (Pacejka, 2006).

The a_{vx} cannot provide the peak friction coefficient directly (Figure 4). However, if the maximum possible acceleration on a given road surface is known, the information may be utilized to understand the road surface μ* and to specify the optimal wheel slip accordingly (Table 2).

In heavy braking maneuver, the driver requests a peak braking torque by slamming on a brake pedal. During the first time lapse of the braking maneuver, the ABS is not yet activated, and this interval is used for maximum a_{vx} detection. Therefore, the peak measured deceleration rate is referred to an appropriate road surface from Table 2. As soon as the road is estimated, the controller identifies an optimal wheel slip for a given road surface (Table 2), and the ABS control is running. A road surface detection example for wet and icy roads is presented in Figure 6. The controller detects a maximum deceleration rate and tries to maintain it during the whole braking maneuver by holding an optimal wheel slip.

Apart from this, to understand if the road surface has changed during the maneuver, the value of maximum a_{vx} resets to zero every 0.3 seconds. While μ* resets, a top braking torque is requested again. While the total torque grows, the algorithm records the new peak of a_{vx}. Thus, if the road surface has not been changed, approximately the same deceleration peak as in the previous step is fixed. However, if the road surface is

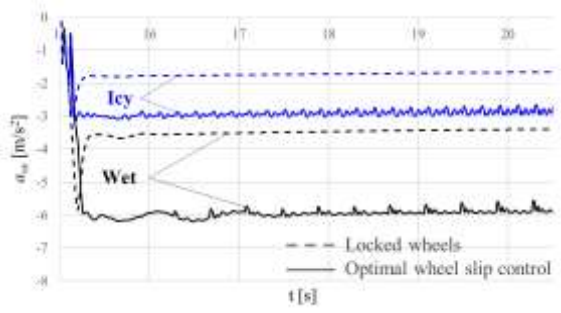

Figure 6. Vehicle longitudinal deceleration with locked wheels and with optimal slip control on wet and icy road surfaces.

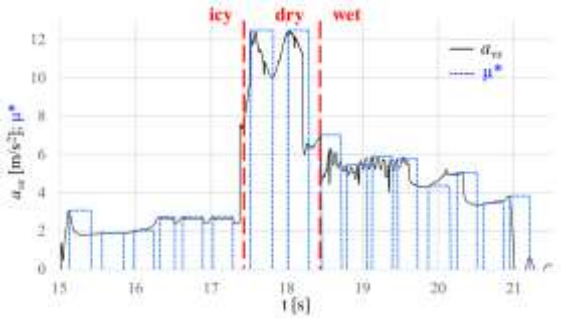

Figure 7. An example of road surface estimation in braking on varying road surfaces from icy, dry to wet profiles.

different from the one in previous step, a new maximum value of a_{vx} is noted.

Figure 7 illustrates the principle of the proposed technique for braking performance. The black line represents vehicle a_{vx}. The blue dotted line indicates estimated road surface μ* for varying roads from icy to dry and to wet. More information about the controller performance on varying road surfaces can be found in (Aksjonov *et al.*, 2016). In next Section, where the simulation results are presented, it can be seen that the wheel slip do not rise significantly while the μ* resets. Consequently, the road surface estimation method has no effect on the vehicle lateral control maintenance.

To guarantee controller robustness to other roads, it is not enough to have the information about λ and μ* exclusively on dry, wet and icy surfaces. In reality, the drivers deal with a variety of different environment conditions. For instance, the optimal slips for dry concrete or snow roads are not the same as for the dry or icy surfaces, respectively (Doumiati *et al.*, 2013). Besides, the tire forces for the worn and new tire on the same road have different behavior (Pacejka, 2006).

In our case, it is not necessary to collect a huge amount of data for different road surfaces. It is enough to study the most common ones (e.g. dry, wet, icy). Based on their tendency, the controller can be designed as an artificial decision making system using fuzzy logic. On the contrary, the conventional control applications are not suitable for nonlinear plant control with uncertain knowledge and measurement or without mathematical model (Passino and Yurkovich, 1998; Reznik, 1997).

The fuzzy set theory allows to cover the unknown workspace of the road surfaces and their optimal slip rates (Figures 4). For example, if the road surface is neither wet nor icy, but has a tire behavior somewhere in the middle, it is not efficient to maintain optimal slip exactly for wet or for icy roads. In this case, the amount of braking torque must be applied to hold the optimal slip value also somewhere between wet and icy surfaces.

The FLC, rather than conventional controllers, is capable to deal with the type of information that is partly true and partly false to any degree at the same time (partly icy and partly wet). It is easily understandable to human due to its attempt to model humans' sense of words, decision making and common sense (Negnevitsky, 2005). Its linguistic reasoning may be applied as follows: **IF** *a vehicle peak deceleration rate is somewhere between wet and icy road*, **THEN** *hold an optimal wheels slip value somewhere between wet and icy road*.

In this work, the FLC is chosen due to its ability to discern vague information about other possible road surfaces. The FLC is designed for both the friction and the regenerative ABS controllers with wheel slip λ and estimated road surface μ* as the input signals. The FLC design is described below.

4.2. Fuzzy Logic Controller Design

An FLC may have multiple inputs and outputs. The input numerical signals are traditionally called ''crisp'' and translated into the fuzzy sets through the fuzzification process. The fuzzy set, in its turn, is a pair consisting of an element in universe of discourse (UOD) and a degree of membership function (MF). The rule−base block stores a linguistic knowledge, which is used to convert the fuzzy input sets into the fuzzy output sets by the inference engine. The fuzzy set outputs are then turned back to the real numbers via defuzzification.

An electric motor is faster than a hydraulic actuator. Thus, for the electric motor FLC, Gaussian (exponential) shape MFs are applied. The regenerative braking control variables MFs are presented in Figure 8. The MFs overlap between each other over the whole UOD. A symmetric dispersion guarantees equal sensitivity of the controllers. The triangular MFs chosen

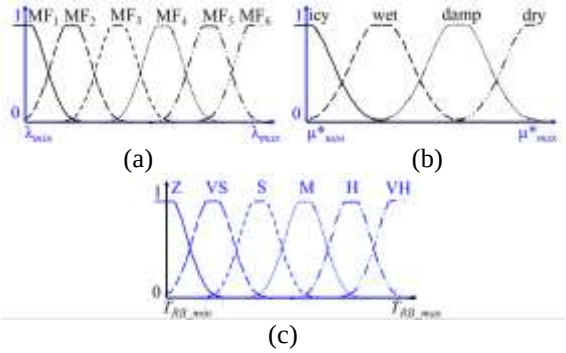

(a) (b) (c)

Figure 8. Regenerative braking fuzzy logic controller MFs: (a) λ input; (b) μ* input; (c) T_{RB} output with a set of MF values {zero (Z), very small (VS), small (S), medium (M), high (H), very high (VH)}.

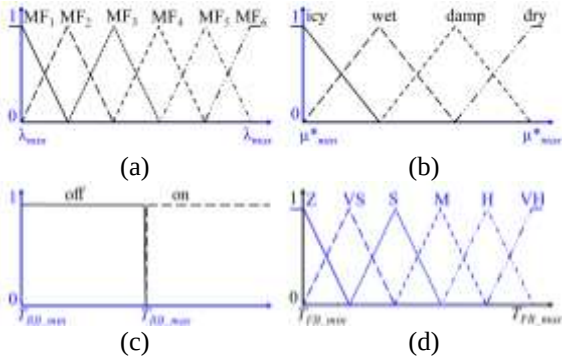

(a) (b) (c) (d)

Figure 9. Friction braking FLC MFs: (a) λ input; (b) μ* input; (c) T_{RB} input; (d) T_{FB} output with a set of MF values {zero (Z), very small (VS), small (S), medium (M), high (H), very high (VH)}.

Table 3. Fuzzy regenerative ABS control rule-base.

μ* \ λ	MF$_1$	MF$_2$	MF$_3$	MF$_4$	MF$_5$	MF$_6$
Icy	VS	Z	Z	Z	Z	Z
Wet	M	S	VS	Z	Z	Z
Damp	VH	H	M	S	VS	Z
Dry	VH	VH	VH	H	S	Z

for the mechanical system control are qualified by fast response because of their narrow shape (Figure 9).

In the FLC design, the input and output variables of the controllers must have a closed frontier [*min*, *max*] of the UOD. For the λ inputs the bounds for the front and rear wheels are chosen according to the tire stable region (Figure 4). This approach is valid because it affords an optimal slip control for almost every studied road surface. The road friction μ* UOD limitations obtained during the vehicle parameterization are described in Section 3.

The μ* input has 4 MFs (Figure 8b, 9b) with UOD restriction narrowed in [3, 12]. An additional input of the friction braking controller acquires an activation signal, which has only 2 MFs (Figure 9c). This input turns on the friction braking system, when the regenerative braking FLC output signal reaches its maximum value.

The maximum pressure of the friction brake and the maximum torque of the generator are known from the EV datasheet. Thus, the UODs of the output variables lay between [0, 151] and [0, 200], correspondingly. Each output variable has 6 MFs (Figure 8c, 9d).

The controllers have a multiple input, single output (MISO) structure. Taken from (Passino and Yurkovich, 1998) MISO pattern of the FLC linguistic rules in modus ponens form (**If**−**Then**) for the regenerative ABS is as follows:

$$\textbf{If } u_1 \text{ is } A^j_1 \textbf{ and } u_2 \text{ is } A^k_2 \textbf{ Then } y_q \text{ is } B^p_q, \qquad (16)$$

where u_1 and u_2 denote the FLC inputs λ and μ*, respectively; y_q denotes the controller output torque; A^j_1 and A^k_2 relate to the j^{th} and k^{th} linguistic value related to wheel slip and road surface, respectively; and B^p_q is the linguistic value of the output torque.

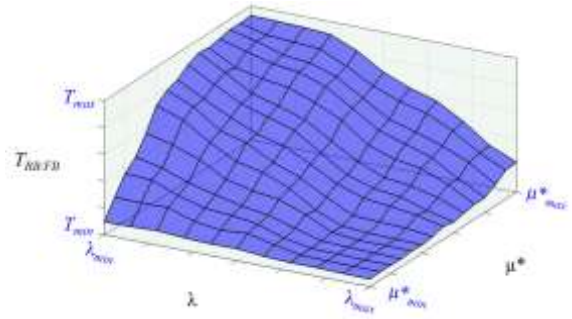

Figure 10. Regenerative ABS FLC surface.

Table 4. Fuzzy logic controller design outlook.

Parameter	Regenerative braking	Friction braking
Structure	MISO	MISO
Crisp input	Slip λ (6 MFs) Road condition μ* (4 MFs)	Slip λ (6 MFs) Road condition μ* (4 MFs) Regenerative brake torque T_{RB} (2 MFs)
Crisp output	Regenerative brake torque T_{RB} (6 MFs)	Friction brake torque T_{FB} (6 MFs)
Fuzzy conjunction	AND = *min* (λ, μ*)	AND = *min* (λ, μ*, T_{RB})
MFs	Gaussian Symmetric	Linear Symmetric
Inference method	Mamdani´s	Mamdani´s
Rule−base	24 Modus Ponens	25 Modus Ponens
Implication operation	*min* (T_{RB})	*min* (T_{FB})
Aggregation method	*max* (T_{RB})	*max* (T_{FB})
Defuzzification	Geometric centre	Geometric centre

Table 3 shows the linguistic relation between the controller inputs and output. The rules are true for both the friction and the regenerative braking FLCs. In total, 24 rules are used for regenerative braking control, while 25 rules are utilized for mechanical friction brake. A controller activation signal represents an additional rule in the friction actuator. The Mamdani's inference mechanism is applied.

The rule−base is designed to keep an optimal wheel slip by providing a necessary braking torque on every road surface. When the slip is higher than its optimal value, the torque diminishes. When the slip value is lower, the torque increases. For example, for the wet road the optimal wheel slip is between 7 − 8%, which is somewhere between MF$_2$ and MF$_3$ depending on the front or rear wheels. A preliminary study (Section 3) has shown that to hold this value, approximately 1300 Nm and 750 Nm torques are required for front and rear wheels, respectively. The torque corresponds to "small (S)" and "very small (VS)" output MFs. When the slip value is higher, the torque decreases. When the slip value is lower, the torque rises. The same logic in linguistic rules is true for other road surfaces.

Fuzzy reasoning ends up with defuzzification procedure. The decoupled ABS controller defuzzification is calculated using the center−of−gravity approach. This method is chosen based on the authors' experience and good continuity and plausibility. The three−dimensional surface of the designed FLC is expressed in Figure 10.

Each of the 4WDs is controlled independently. Altogether, four controllers are designed for the regenerative braking ABS: front and rear wheels regenerative braking, front and rear wheels friction

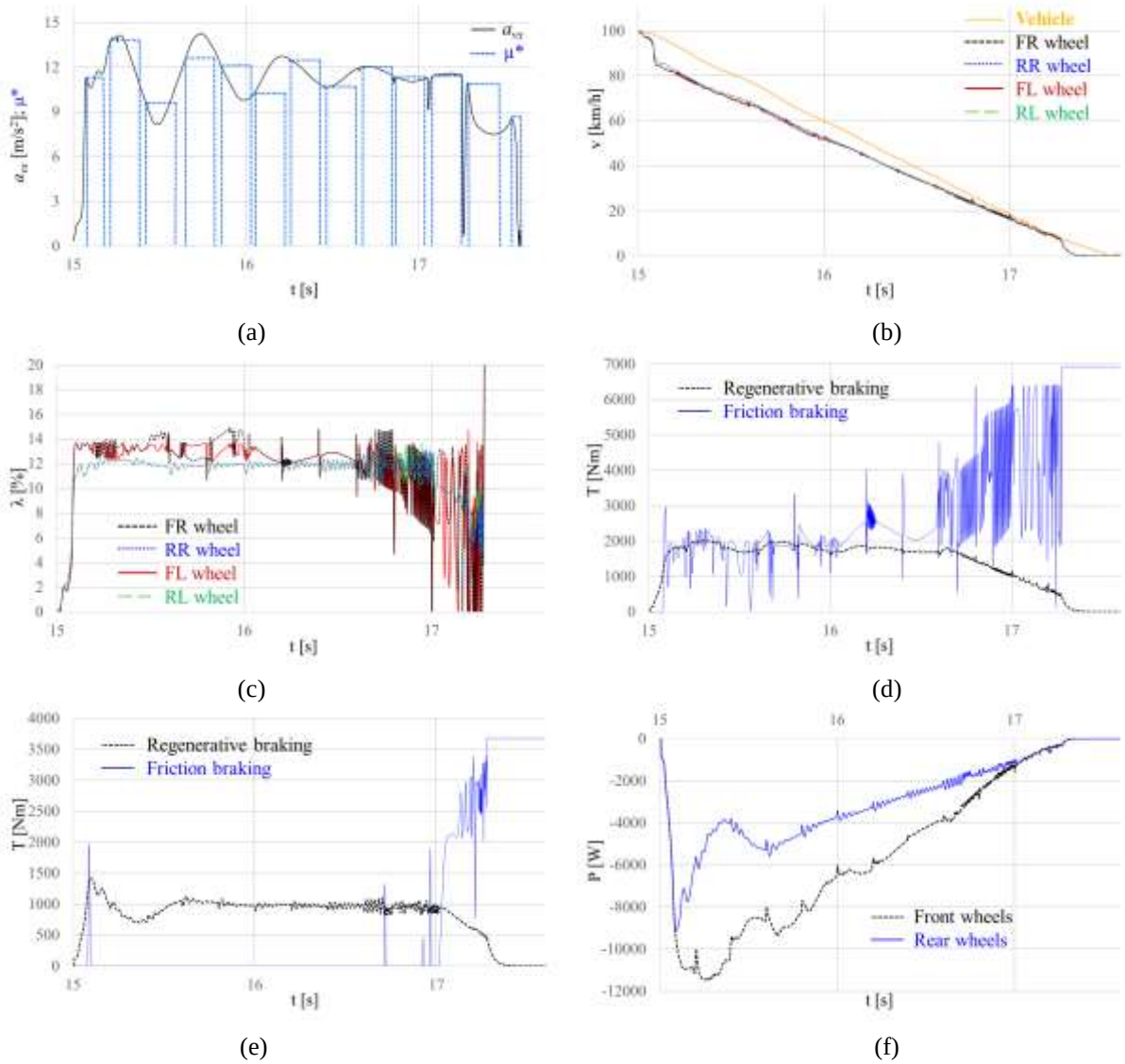

Figure 11. Regenerative braking on a straight dry asphalt road surface: (a) road surface estimation; (b) velocity curves; (c) wheel longitudinal slip curves; (d) front wheels braking torque curves; (e) rear wheels braking torque curves; (f) power dissipation curves.

braking FLCs. The outlook of the designed for the regenerative and friction braking ABS FLCs is summarized in Table 4.

5. RESULTS

Simulation results conducted on a straight road are presented in this section. The vehicle is accelerated to 100 km/h and then the heavy braking is applied. The results are introduced as a comparison between decoupled regenerative ABS control, only mechanical friction ABS control, and pure wheel blocking deceleration. Different road surfaces (i.e. dry, wet, icy) are examined to study the control method ability to maintain an optimal wheel slip ratio.

The regenerative ABS control simulation results on the straight dry asphalt road are studied in this section in details (Figure 11). The road surface estimation is introduced in Figure 11a. At around 15.1 seconds, the controller measures the first peak of a_{vx}. This value is almost 12 m/s^2. Referring to Table 2 (peak a_{vx} for dry road is 11.78 m/s^2), the controller reveals vehicle deceleration on a dry road. Herewith, the optimal slip value for each wheel for a dry asphalt is detected (Table 2). The road surface estimation procedure continues upon the fixed frequency until the ABS deactivation.

Table 5. ABS braking performance comparison on different road surfaces.

Road \ Criterion	Type	s [m]	$a_{average}$ [m/s^2]	ABS_{IP}	i	$\lambda_{average}$ [%]	λ_e [%]	P_{reg} [%]	E_c[kJ]
Dry	Regenerative brake	32.99	−11.40	1.50	FL	11.79	1.39	6.24	27.19
					FR	11.79	1.39	6.10	27.19
					RL	11.32	0.99	9.25	32.83
					RR	11.32	0.99	9.26	32.83
	Friction brake	33.15	−11.37	1.49	FL	11.53	1.65	0	40.31
					FR	11.52	1.65	0	40.31
					RL	10.87	1.44	0	40.31
					RR	10.94	1.37	0	40.31
	Pure wheel blocking	51.30	−7.62	–	FL	100	-	0	40.31
					FR	100	-	0	40.31
					RL	100	-	0	40.31
					RR	100	-	0	40.31
Wet	Regenerative brake	64.48	−5.92	1.93	FL	8.70	0.36	9.47	22.57
					FR	8.70	0.36	9.47	22.57
					RL	8.13	1.01	9.52	29.45
					RR	8.13	1.01	9.52	28.82
	Friction brake	66.15	−5.83	1.90	FL	9.04	0.70	0	40.31
					FR	9.03	0.69	0	40.31
					RL	8.51	1.39	0	40.31
					RR	8.51	1.39	0	40.31
	Pure wheel blocking	110.04	−3.07	–	FL	100	-	0	40.31
					FR	100	-	0	40.31
					RL	100	-	0	40.31
					RR	100	-	0	40.31
Icy	Regenerative brake	130.97	−2.85	1.74	FL	6.28	0.14	10.27	24.14
					FR	6.28	0.14	10.27	24.14
					RL	5.82	0	9.75	27.36
					RR	5.82	0	9.75	27.36
	Friction brake	132.29	−2.80	1.70	FL	6.43	0.29	0	40.31
					FR	6.43	0.29	0	40.31
					RL	5.58	0.24	0	40.31
					RR	5.59	0.23	0	40.31
	Pure wheel blocking	226.03	−1.64	–	FL	100	-	0	40.31
					FR	100	-	0	40.31
					RL	100	-	0	40.31
					RR	100	-	0	40.31

The wheels and vehicle speed curves are viewed in Figure 11b. At the time about 17.2 seconds the ABS control is turned off, because the vehicle speed reaches 8 km/h. The road estimation also stops. The maximum mechanical braking pressure is then applied and the wheels are immediately locked for an insignificantly short period.

The wheel slip plots are shown in Figure 11c. The difference in the slip value for the front and the rear wheels can be easily recognized. Optimal slip deceleration on the dry surface is maintained during the whole braking process, because the road surface is uniform.

Braking torque curves for front and rear wheels are introduced in Figure 11d and Figure 11e, accordingly. Both the regenerative and mechanical friction torque curves are shown in the same charts. At 15.1 seconds, the total braking torque (a sum of regenerative and mechanical torques) on both wheels is maximum, because the controller measures peak vehicle deceleration, and the ABS is not yet turned on.

For the front wheels, the torque generated by the SRMs is not enough to retain the optimal wheel slip

value. As a result, the controller requests additional torque from the mechanical brakes to maintain optimal slip deceleration (Figure 11c). Both regenerative and friction brakes work simultaneously. However, the electric motors do not supply constant torque within the whole braking maneuver. In around 16.7 seconds, the generators due to their efficiency limit (Figure 3) diminish the torque and the recuperation energy decreases. Contrariwise, the friction braking pressure rises to continue maintaining optimal wheel slip.

For the rear wheels, the mechanical friction braking torque is not actuated, because the SRM's one is enough to retain the optimal slip for the rear wheels on a dry road. Likewise, for the front wheels, the motor stops recycling kinetic energy on low speeds due to the SRM characteristics. Therefore, with low wheel velocities, the friction brakes are also activated.

An SRM power dissipation is performed in Figure 11f. The negative amount of power shown is the energy recuperated during the vehicle deceleration for only one rear or front wheel. The power saved by the front wheel is greater than the one by the rear wheel.

A comparison between regenerative strategy and only friction braking on different road surfaces, including icy, wet and dry is shown in Table 5. The friction braking is also designed to retain the optimal wheel slip. For the dry road, the front wheels (9%) do not recover as much energy as the rear wheels (6%). This is due to the higher overall torque demand for required wheel slip braking. The rest of the necessary torque for front wheels is compensated by the friction brake, which is almost as high as the generator's one (Figure 11d). Accordingly, the effectiveness of energy regeneration on the dry surface is not exalted as, for instance, braking on a wet or icy surfaces, where only motor torque is enough to decelerate the car with the optimal wheel slip.

For the icy and wet roads, front and rear wheels recuperation is equal, because only the SRM is applied to stop the vehicle. Hence, the brake pads wear is minimum and the brakes particle emission is also belittled. Each wheel saves around 10% of the whole energy spent on transport deceleration. Eventually, the control method maintains an optimal slip ratio for each studied road surface individually, what promises robust and energy efficient vehicle deceleration and lateral dynamics control preservation.

In modern vehicles, the controllers keep the slip around 20%. This threshold is optimal individually for a dry asphalt surface. An optimal slip for icy road is usually more than two times smaller (Figure 4) and the threshold of 20% consequently leads to more than 50% energy losses. With the reference slip control, the energy losses are also true for other roads, like wet, snow or damp. As with the proposed control method, a wheel slip deceleration optimal for varying road surfaces guarantees an improvement of energy efficiency. The studied in this paper decoupled regenerative and friction braking ABS FLC distributes torque between 4WD powertrain wheels to maintain an optimal wheel slip for every road surface.

However, the average slip values are different, when comparing regenerative and friction brakes. The difference between theoretical (Table 2) and calculated during the simulation experiment slip λ_e for each wheel is presented in Table 5. The smaller the difference, the higher the accuracy in slip control is accomplished.

Although the controllers for electric and hydraulic systems are identical, the regenerative ABS FLC holds the wheel slip values closer to the optimal for a given tire model (Table 2), thus, λ_e is lower. It evidences that the electric actuators' reaction is faster than the mechanical one, what allows the precise wheel slip control. What is more, the smaller the error in wheel slip control, the shorter the braking distance is achieved (Table 5) due to higher braking force (Rajamani, 2012).

For the modelled SUV EV, the proposed control method allows to save around 10% of the whole energy required for the fast and simultaneously safe deceleration, what is maximum for a given SRM. Thanks to the recuperative braking technology, energy consumption in each studied case is smaller for the decoupled system, comparing to the pure friction or braking with blocked wheels. Therefore, the regenerative ABS control method opens a possibility for energy improvement, what is an essential problem in environmental sustainability.

6. DISCUSSION

Electric mobility is a promising technology on a way to environmentally sustainable transportation. The EVs have a list of advantages over conventional ICE vehicles, such as quite operation, cheap fuel, and zero emission. In addition, EVs architecture, like individual 4WD powertrain, opens a great opportunity to design accurate, efficient and fast dynamics control methods using different computational intelligence techniques. Nevertheless, EV mobility has also some disadvantages, such as a long recharging time and a short driving distance. The distance range may be increased using the kinetic energy recovery system.

Multiple researches studied in Section 2 show that scholars focused only on ABS (Kathun *et al*., 2003; Chen *et al*., 2010) and ESP control (Tahami *et al*., 2003; Pusca *et al*., 2004; Kim *et al*., 2008) using FLC, or exclusively on regenerative braking algorithms (Paterson and Ramsay, 1993; Peng *et al*., 2006; Li *et al*., 2008; Nian *et al*., 2014; Zhang *et al*., 2016). Other authors merely dedicated the FLC approaches on electric and friction torque blending strategies (Zhang *et*

al., 2009; Xu *et al*., 2011; Jianyao *et al*., 2015). In (Guo *et al*., 2014), the solution depends on a wheel slip threshold. In all these cases, unlike for the FLC described in this paper, the controller robustness and energy efficient deceleration are not proved.

The regenerative braking ABS control method proposed here is directed to illustrate both energy recuperation and vehicle efficient safety fulfilments. The control method has the series architecture, in which electric motor torque is used maximally. The power gained from kinetic energy of the decelerated vehicle is directed to recycle the power back to the storage devices, such as ultracapacitors or directly to the battery cell.

Tire−road adhesive coefficient estimation was performed using fuzzy set theory in (Layne *et al*., 1993; Sharkawy, 2006). The controllers were designed with the slip threshold of 20%. In (Paul *et al*., 2016), the ABS performance was not presented, hence, the vehicle safety is not demonstrated. In this paper, the recuperation braking control method is accompanied with ABS. The control method is designed to identify road adhesion and then to hold the optimal for various road surfaces wheel slip. The controller dependence on reference slip threshold is avoided.

The proposed controller has a certain advantage over earlier introduced similar methods. Namely, in (Paul *et al*., 2016), likewise in this paper, the authors substituted a complex mathematical model for tire-road friction coefficient estimation with simple FLC. However, despite the high energy recuperation the controller did not hold an optimal for various road surfaces wheel slip. Thus, unlike inherent to the FLC described in this paper, a maximum possible efficient deceleration with steerability maintenance is not preserved.

In (Castillo *et al*., 2016), a road type was detected by Kalman filter, FLC, and artificial neural network models combination. In (Ivanov *et al*., 2006), road surface was estimated using eight variables applying three different FLCs. Lastly, another intelligent ABS FLC was described in (Aly, 2010), where three different FLCs (i.e. road identifier, optimal wheel slip estimator, and ABS controller) were connected in series. These controllers show good robustness to varying road surfaces. However, they are, unlike the controller proposed in this paper, where a road surface comprehension is accomplished referring to only single variable, vehicle body peak deceleration, very complex and computationally expansive. In addition, the algorithms were designed only for on a conventional hydraulic braking system. The appliance on the electric actuators and decoupled system were not stressed.

In suggested in this paper FLC, when the torque generated by the SRM is not enough to keep an optimal slip for a given surface, the controller runs the conventional friction brakes. Torque blending as well as regenerative energy capability are embodied based on fuzzy sets theory for each wheel separately. The controller outcomes are studied on a different road surfaces and are compared with the ABS control without regenerative possibility and with locked wheels deceleration.

A 10DOF vehicle model with a visual simulation interface helps to comprehend the vehicle behavior under various conditions. Analyzing the simulation outcomes in Section 5, it is concluded:

- the proposed solution recovers in average 8% of power for each wheel, when on the wet and icy surfaces the energy consumption is lower;
- the control method maintains the optimal wheel slip value for varying road surfaces (Figure 4);
- electric actuators are faster than mechanical one, what enables them to maintain more accurate wheel slip control.

Additionally, the results have shown that with the designed control method the friction brakes are used less in EV. The time of friction between pads and discs is decreased, and thus the brake pads wear is minimized. It reduces at the same time the vehicle maintenance cost, brake components wear, and brake pads particles emission (El−Garhz *et al*., 2013).

7. CONCLUSION

In short, the research innovations in recuperation ABS control stressed in this paper are listed as follows:

- road surface recognition from vehicle longitudinal deceleration with optimal wheel slip for different road surface braking performance and high efficiency kinetic energy recovery based on FLC;
- control method verification on 10DOF SUV EV mathematical model parametrized according to the vehicle manufacturer;
- simulation comparison between decoupled regenerative, pure friction, and locked wheels braking performance on different road surfaces.

The results obtained in current research are limited with numerical simulation. Hence, the additional advantage of the present work is that it opens a great opportunity for further research. For instance, the controller could be tested on a hardware−in−the−loop system or on a real vehicle, because different behavior is expected for simulation and real world environments.

Due to missing information, state−of−charge, battery temperature, and some other aspects of power consumption are neglected in the model described in this paper. The future research will cover a study of the controller effectiveness on an extended model, where the mentioned characteristics have to be taken into consideration. Similarly, different maneuvers, for example, braking while cornering, may be also studied.

Finally, although the controller outputs are restricted by the system physical parameters (maximum motor current and maximum pressure), the controller nonlinear stability analysis may be performed, such as the Lyapunov's direct method proved to be very efficient in FLC stability analysis (Passino and Yurkovich, 1998) (pp. 187−232).

ACKNOWLEDGEMENT–This work was supported by the European Community Horizon 2020 Framework Programme under the Marie Skłodowska−Curie grant agreement (grant number 675999); and the Deutschen Bundesstiftung Umwelt (DBU) exchange scholarship.

REFERENCES

Acosta, M. and Kanarachos, S. (2017). Tire lateral force estimation and grip potential identification using neural networks, extended Kalman filter, and recursive least square. *Neural. Comput. & Appilc*., 1−21.

Aksjonov, A., Augsburg, K. and Vodovozov, V. (2016). Design and simulation of the robust ABS and ESP fuzzy logic controller on the complex braking maneuvers. *Appl. Sci*. **6**, **12**, 382−390.

Aly, A. A. (2010). Intelligent fuzzy control for antilock brake system with road−surfaces identifier. *Proc. of 2010 IEEE Intern. Conf. on Mechat. & Automation (ICMA)*, Xi'an, China.

Bansal, R. C. (2005). *Electric Vehicles*, in: Emadi, A. (Ed.) *Handbook of Automotive Power Electronics and Motor Drives*. Taylor and Francis Group, Boca Raton, FL, USA, 55−96.

Castillo, J. J., Cabrera, J. A., Guerra, A. J. and Simon, A. A. (2016). Novel electrohydraulic brake system with tire−road friction estimation and continuous brake pressure control. *IEEE Trans. on Ind. Elec*. **63**, **3**, 1863−1875.

Chen, H., Yang, J., Du, Z. and Wang, W. (2010). Adhesion control method based on fuzzy logic control for four−wheel driven electric vehicle. *SAE Inter. J. Passeng. Cars − Mech. Syst.* **3**, **1**, 217−225.

Cikanek, S. R. (1994). *Fuzzy Logic Electric Vehicle Regenerative Antiskid Braking and Traction Control System*. U.S. Patent 5,358,317.

Dhameja, S. (2002). *Electric Vehicle Battery Systems*. Butterworth−Heinemann, Woburn, MA, USA, 1−42.

Doumiati, M., Charara, A., Victorino, A., Lechner, D. (2013). *Vehicle Dynamics Estimation using Kalman Filtering: Experimental Validation*. 2nd ed. ISTE Ltd and John Wiley & Sons, Inc.: Hobokene, UK, 37−61.

Ehret, T. (2014). *Electronic Stability Program (ESP)*, in: Reif, K. (Ed.), *Brakes, Brake Control and Driver Assistance Systems: Function, Regulation and Components*. Springer, Friedrichshafen, Germany, 102−123.

Ehsani, M., Gao, Y., Gay, S. E. and Emadi, A. (2005). *Modern Electric, Hybrid Electric, and Fuel Cell Vehicles*. CRC Press LLC, Boca Raton, FL, USA, 99−116, 204−232, 277−298.

El−Garhy, A. M., El−Sheikh, G. A. and El−Saify, M. H. (2013). Fuzzy life−extending control of anti−lock braking system. *Ain Shams Eng. J.* **4**, **4**, 735−751.

Guo, J., Jian, X. and Lin, G. (2014). Performance evaluation of an anti−lock braking system for electric vehicles with a fuzzy sliding mode controller. *Energies* **7**, **10**, 6459−6476.

Han, K., Hwang, Y., Lee, E. and Choi, S. (2015). Robust estimation of maximum tire-road friction coefficient considering road surface irregularity. *Inter. J. of Automotive Technology* **17**, **3**, 415−425.

Ivanov, V. G., Algin, V. B. and Shyrokau, B. N. (2006). Intelligent control for ABS application with identification of road and environmental properties. *Inter. J. of Vehic. Autom. Sys*. **4**, **1**, 44−67.

Ivanov, V. (2015). A review of fuzzy methods in automotive engineering applications. *Eur. Transp. Res. Rev.* **7**, **29**, 19−29.

Jianyao, H., Huawei, X., Zhiyuan, H., Linyi, H. and Qunxing, L. (2015). Study on braking force distribution based on fuzzy control algorithm. *Proc. of the 2015 IEEE Advanced Inform. Techn., Electronic and Autom. Cont. Conf. (IAEAC)*. Chongqing, China.

Khatun, P., Bingham, C. M., Schofield, N. and Mellor, P. H. (2003). Application of fuzzy control algorithm for electric vehicle antilock braking/traction control systems. *IEEE Trans. on Veh. Tech*. **52**, **5**, 1356−1364.

Kiencke, U. and Nielsen, L. (2005). *Automotive Control Systems: For Engine, Driveline, and Vehicle*. 2nd ed. Springer−Verlag Berlin Heidelberg, Berlin, Germany, 301−350.

Kim, D., Hwang, S. and Kim, H. (2008). Vehicle stability enhancement of four−wheel−drive hybrid electric vehicle using rear motor control. *IEEE Veh. Tech. Soc*. **57**, **2**, 727−735.

Kim, D.−H., Kim, J.−M., Hwang, S.−H. and Kim, H.−S. (2007). Optimal brake torque distribution for a four−wheel−drive hybrid electric vehicle stability enhancement. *Proc. IMechE., Part D: J. of Automobile Engineering* **221**, **11**, 1357−1366.

Koch−Dücker, H.−J. and Papert, U. (2014). *Antilock Braking System (ABS)*, in: Reif, K. (Ed.), *Brakes, Brake Control and Driver Assistance Systems: Function, Regulation and Components*. Springer, Friedrichshafen, Germany, 74−93.

Layne, J. R., Passino, K. M. and Yurkovich, S. (1993). Fuzzy learning control for antiskid braking systems. *IEEE Trans. on Cont. Syst. Tech*. **1**, **2**, 122−129.

Li, X., Xu, L., Hua, J., Li, J. and Ouyang M. (2008). Regenerative braking control strategy for fuel cell hybrid vehicle using fuzzy logic. *Proc. of the 11th Intern. Conf. on Electrical Mach. & Syst., 2008 (ICEM 2008)*, Wuhan, China.

Long, B., Lim, S. T., Ryu, J. H. and Chong, K. T. (2014). Energy-regenerative braking control of electric vehicles using three-phase brushless direct-current motors. *Energies* **7**, **1**, 99−114.

Miller, J. M. (2005). *Hybrid Electric Vehicles*, in: Emadi, A. (Ed.), *Handbook of Automotive Power Electronics and Motor Drives*. Taylor and Francis Group, Boca Raton, FL, USA, 21−36.

Negnevitsky, M. (2005). *Artificial Intelligence: A guide to intelligent systems*. 2nd ed. Addison−Wesley: Harlow, UK, 87−131.

Nian, X., Peng, F. and Zhang, H. (2014). Regenerative braking system of electric vehicle driven by brushless DC motor. *IEEE Trans. on Ind. Elec*. **61**, **10**, 5798−5808.

Pacejka, H. B. (2006). *Tyre and Vehicle Dynamics*. 2nd ed. Butterworth−Heinemann: Oxford, UK, 156−215.

Passino, K. M. and Yurkovich, S. (1998). *Fuzzy Control*. Addison−Wesley Longman, Inc.: Menlo Park, California, CA, USA, 1−22, 23−118, 187−232.

Paterson, J. and Ramsay, M. (1993). Electric vehicle braking by fuzzy logic control. *Proc. of the Conf. Record of the 1993 IEEE Industry Applic. Soc. Annual Meeting*, Toronto, Canada.

Paul, D., Velenis, E., Cao, D. and Dobo, T. (2016). Optimal μ−estimation based regenerative braking strategy for an AWD HEV. *IEEE Trans. on Transp. Elect*. **3**, **1**, 1−10.

Peng, D., Zhang, J. and Yin, C. (2006). Regenerative braking control system improvement for parallel hybrid electric vehicle. *Proc. of the Intern. Techn. and Innov. Conf. (ITIC 2006)*, Hangzhou, China.

Pusca, R., Ait−Amirat, Y., Berthon, A. and Kauffmann, J. M. (2004). Fuzzy−logic−based control applied to a hybrid electric vehicle with four separate wheel drives. *IEE Proc. Con. Theo. and Appl.* **151**, **1**, 73−81.

Rajamani, R. (2012). *Vehicle Dynamics and Control*. 2nd ed. Springer: New York, USA, 87−112.

Rath, J. J., Veluvolu, K. C. and Defoort, M. (2015). Simultaneous estimation of road profile and tire road friction for automotive vehicle. *IEEE Trans. on Veh. Tech*. **64**, **10**, 4461−4471.

Reznik, L. (1997). *Fuzzy Controllers*. Butterworth-Heinemann Newnes: Oxford, UK, 1−18.

Savitski, D., Augsburg, K. and Ivanov, V. (2014). Enhancement of energy efficiency, vehicle safety and ride comfort for all−wheel drive full electric vehicles. *Proc. of the Euro. Braking Techn. Conf. & Exhib. (EuroBrake 2014)*, Lille, France.

Savitski, D., Ivanov, V., Shyrokau, B., Pütz, T., De Smet, J. and Theunissen, J. (2016). Experimental investigations on continuous regenerative anti−lock braking system of full electric vehicle. *Inter. J. of Automotive Technology* **17**, **2**, 327−338.

Sharkawy, A. B. (2006). Genetic fuzzy self−tuning PID controllers for antilock braking systems. *Alexandria Eng. J.* **45**, **6**, 657−673.

Tahami, F., Kazemi, R. and Farhanghi, S. (2003). A novel driver assist stability system for all−wheel−drive electric vehicles. *IEEE Veh. Tech. Soc*. **52**, **3**, 683−692.

Xia, X., Xiong, L., Sun, K. and Yu, Z. P. (2016). Estimation of maximum road friction coefficient based on Lyapunov method. *Inter. J. of Automotive Technology* **17**, **6**, 991−1002.

Xiong, L. and Yu, Z. (2011). *Vehicle Dynamics Control of 4 In−Wheel−Motor Drived Electric Vehicle*, in: Soylu, S., (Ed.) *Electric Vehicles − Modelling and Simulation*. InTech, Rijeka, Croatia, 67−106.

Xu, G., Li, W., Xu, K. and Song, Z. (2011). An intelligent regenerative braking strategy for electric vehicles. *Energies* **4**, **9**, 1461−1477.

Ye, M., Jiao, S. and Cao, B. (2010). Energy recovery for the main and auxiliary sources of electric vehicles. *Energies* **3**, **10**, 1673−1690.

Zabler, E. (2014). *Sensors for Brake Control*, in: Reif, K. (Ed.), *Brakes, Brake Control and Driver Assistance Systems: Function, Regulation and Components*. Springer, Friedrichshafen, Germany, 142−153.

Zhang, J., Song, B., Cui, S. and Ren, D. (2009). Fuzzy logic approach to regenerative braking system. *Proc. of the 2009 Intern. Conf. on Intellig. Hum.−Mach. Sys. & Cybern*., Hangzhou, China.

Zhang, X., Wang, Y., Liu, G. and Yuan, X. (2016). Robust regenerative charging control based on T−S fuzzy sliding−mode approach for advanced electric vehicle. *IEEE Trans. on Transp. Elect*. **2**, **1**, 52−65.